Optical trapping of a spherically symmetric sphere in the ray-optics regime: a model for optical tweezers upon cells

Yi-Ren Chang, Long Hsu, and Sien Chi

Since their invention in 1986, optical tweezers have become a popular manipulation and force measurement tool in cellular and molecular biology. However, until recently there has not been a sophisticated model for optical tweezers on trapping cells in the ray-optics regime. We present a model for optical tweezers to calculate the optical force upon a spherically symmetric multilayer sphere representing a common biological cell. A numerical simulation of this model shows that not only is the magnitude of the optical force upon a Chinese hamster ovary cell significantly three times smaller than that upon a polystyrene bead of the same size, but the distribution of the optical force upon a cell is also much different from that upon a uniform particle, and there is a 30% difference in the optical trapping stiffness of these two cases. Furthermore, under a small variant condition for the refractive indices of any adjacent layers of the sphere, this model provides a simple approximation to calculate the optical force and the stiffness of an optical tweezers system. © 2006 Optical Society of America

OCIS codes: 140.7010, 170.4520, 080.2720.

1. Introduction

Since Ashkin *et al*. first trapped a micrometer-sized bead with a focused laser by a high numerical aperture microscopic objective[1] in 1986, optical tweezers have become a famous technique of trapping, sorting, and assembling microparticles and nanoparticles. Especially in cellular and molecular biology, optical tweezers are also convenient for manipulating cells in the microscale[2–4] and for measuring the biological force of molecular interactions.[5,6] To describe the trapping mechanism of optical tweezers, thus far there are two major models: a ray-optics model by Ashkin[7] and a dipole-limit model by Harada and Asakura.[8] The ray-optics model is valid as the radius of the trapped particle is ten times larger than the wavelength of the laser. However, the dipole-limit model is also valid as the radius of the trapped particle is much smaller than the wavelength of the laser. There are also other models dealing with particles, whose radius is near the wavelength of the laser.[9–11] Nevertheless, all the mentioned models assume that the trapped particle has a uniform refractive index. Unfortunately, this assumption is not true for biological cells. On the other hand, although there is some recent work on a nonuniform refractive index,[12] it is not easy to directly obtain an optical force upon a biological cell due to the complex calculation with those models. In this regard, we recently introduced a simple model for optical tweezers upon a single cell in the regime of the dipole-limit model.[13] This is indeed an extension of the dipole-limit model, in which a biological cell is simplified as a nonuniform Rayleigh sphere with a spherically symmetric refractive index. However, this extended dipole-limit model does not fit for larger cells. Complementarily, in this paper, we further propose an extension of the ray-optics model for optical tweezers upon a single cell in the ray-optics regime.

According to Ashkin's ray-optics model,[7] the optical trapping force arises from the momentum transfer between photons and the trapped particle. Therefore in this extended ray-optics model, we also consider the focused laser beam out of an objective then into a cell as a bundle of rays, each of which consists of a series of photons. Similar to the nonuniform cell in our extended dipole-limit model,[13] we assume the cell to be a multilayer sphere with a spherically symmetric refractive index as well. Similarly, as the thickness of each layer and the variation of the refractive

Y.-R. Chang (YRChang.eo91g@nctu.edu.tw) and S. Chi are with the Department of Photonics and Institute of Electro-Optical Engineering, National Chiao Tung University, 1001 Ta Hsueh Road, Hsinchu 300, Taiwan. L. Hsu is with the Department of Electrophysics, National Chiao Tung University, 1001 Ta Hsueh Road, Hsinchu 300, Taiwan. S. Chi is also with the Department of Electrical Engineering, Yuan Ze University, 135 Far-East Road, Chung-Li, Taoyuan, Taiwan.

Received 6 April 2005; revised 29 July 2005; accepted 29 July 2005.

0003-6935/06/163885-08$15.00/0

© 2006 Optical Society of America

indices of adjacent layers are infinite small, the sphere is supposedly equivalent to a common biological cell. Therefore the optical trapping force upon the nonuniform cell can be obtained by calculating the momentum-transfer rate due to the overall reflection and the overall refraction of the focused incident rays into the multilayer sphere.

In Section 2 we will explain our extended ray-optics model in detail. We begin with the trace of an incident ray into a multilayer sphere and the corresponding reflections and the refractions at every interface between any adjacent layers. Then we end up with an overall reflection and an overall refraction of the incident ray. According to momentum conservation, this results in an optical force upon the sphere induced by this single incident ray. By integrating all the optical force induced by the bundle of rays of a focused laser beam, we obtain the total optical force of an optical tweezers system. In addition, under a small variant condition for the refractive indices of any adjacent layers of the sphere, we may simplify the complicated derivation of optical force for such a multilayer sphere.

Finally, in Sections 3 and 4 we will examine our extended ray-optics model by applying it to four samples of the same size. In this exercise, a real Chinese hamster ovary (CHO) cell of two layers is used as the nonuniform sphere. On the other hand, a virtual CHO cell of a single layer, a silica bead, and a polystyrene bead are used as the uniform spheres. The selection of the four samples is simply due to the availability of the information on their structures and distributions of refractive indices. We will compare and discuss the difference in magnitude between the trapping force upon a uniform sphere and that upon a nonuniform cell of the same size.

2. Theoretical Analysis

In our extended ray-optics model of optical tweezers for cells, we consider a laser beam focused into a spherically symmetric sphere of multiple layers. The optical trapping force $\mathbf{F}_{opt}$ upon the multilayer sphere can be derived from the resulting overall reflections and refractions of the incident rays according to the momentum-conservation law[7]:

$$\mathbf{F}_{\text{opt}} = \frac{h}{\lambda_{\text{med}}} \left(\sum \mathbf{p}_i - \sum \mathbf{p}_{\text{scat}} \right), \tag{1}$$

where h is Planck's constant, λ_{med} is the wavelength of the focused light in the surrounding medium, $\mathbf{p}_i$ is the photon flux of the incident ray, and $\mathbf{p}_{\text{scat}}$ is the photon flux of the scattered ray that includes the reflections or the refractions of the incident rays.

A. Optical Force Induced by a Single Ray

For simplicity, we assume a nonuniform cell as an N-layer sphere of radius r_N with a spherically symmetric refractive index. Consider a ray incident into this sphere at a vertical distance d, as illustrated in Fig. 1(a), in which the subscript k in this figure refers to the kth layer. Suppose that the radius r_k and the refractive index n_k of every concentric layer are known. The next step is to derive the corresponding reflection and refraction at each interface.

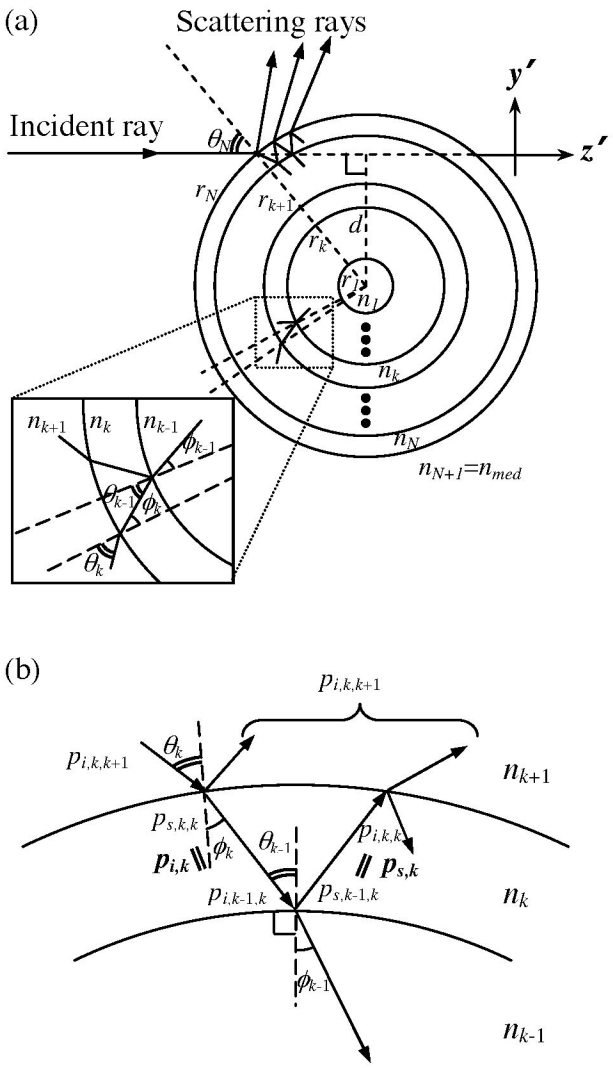

Fig. 1. Scattering schemes of (a) a single incident ray scattered by the proposed multilayer spherically symmetric sphere and (b) the photon fluxes between the $(k-1)$th, kth, and $(k+1)$th layers.

To simplify the derivation, we adapt a complex notation for the photon flux, p, whose real and imaginary parts represent the components of p along z' and y', respectively. As a result, the amplitude and phase of the "complex" p correspond to its magnitude and angle in real space. Consequently, it can be shown that the relationship between an incident photon flux p_0 and its reflection photon flux p_{refl} and refraction photon flux p_{refr} can be written in the forms

$$p_{\text{refl}} = p_0 R \exp(i\Delta\theta_{\text{refl}}) \tag{2}$$

$$p_{\text{refr}} = p_0(1-R)\exp(i\Delta\theta_{\text{refr}}), \tag{3}$$

where R is the reflection rate at the interface, and $\Delta\theta_{\text{refl}}$ and $\Delta\theta_{\text{refr}}$ are the deviation angles of p_{refl} and p_{refr} off the incident photon flux p_0, respectively.

A detailed scheme of reflection and refraction at an arbitrary interface is shown in Fig. 1(b). In this work, at the interface, we consider the incident photon flux as the total incident photon flux into the adjacent layer, and the scattered photon flux as the total scattered photon flux. Furthermore, there are four total photon fluxes associated with the kth interface, which is between the kth layer and the $(k + 1)$th layer. Among them, $p_{i,k,k}$ and $p_{s,k,k}$ are the total incident and the total scattered photon fluxes in the kth layer, respectively. In addition, $p_{i,k,k+1}$ and $p_{s,k,k+1}$ are the total incident and the total scattered photon fluxes in the $(k + 1)$th layer. Note that the subscript here consists of three elements. The first element, i or s, reflects that the photon flux is incident scattered, the second element shows which interface the photon flux is associated with, and the last element describes the layer that the photon flux is in. Also, it can be shown that both $p_{s,k,k}$ and $p_{s,k,k+1}$ can be expanded in terms of the remaining two photon fluxes, $p_{i,k,k}$ and $p_{i,k,k+1}$, as given by

$$p_{s,k,k} = p_{i,k,k}R_k \exp[i(-\pi + 2\phi_k)] + p_{i,k,k+1} \times (1 - R_k)\exp[-i(\theta_k - \phi_k)], \quad (4)$$

$$p_{s,k,k+1} = p_{i,k,k}(1 - R_k)\exp[-i(\theta_k - \phi_k)] + p_{i,k,k+1}R_k \exp[i(\pi - 2\theta_k)], \quad (5)$$

where R_k is the refractive rate at the kth interface. Furthermore, from Snell's law it can be shown that θ_k and ϕ_k can be related to the initial incident angle θ_N in the forms, respectively,

$$\sin\theta_k = \frac{r_{k+1}}{r_k}\sin\phi_{k+1} = \frac{r_{k+1}}{r_k}\frac{n_{k+2}}{n_{k+1}}\sin\theta_{k+1} = \frac{r_N}{r_k}\frac{n_{N+1}}{n_{k+1}}\sin\theta_N, \quad (6)$$

$$\sin\phi_k = \frac{n_{k+1}}{n_k}\sin\theta_k = \frac{r_N}{r_k}\frac{n_{N+1}}{n_k}\sin\theta_N, \quad (7)$$

where $\sin\theta_N = d/r_N$.

Additionally, we further assume that the refractive indices of all layers are real, so that there will be no photon flux loss when the rays pass in any layer of the sphere. In other words, the photons scattered from the $(k - 1)$th interface would all become the incident photons into the kth interface. This results in $p_{i,k,k} = p_{s,k-1,k}$ and similarly $p_{s,k,k} = p_{i,k-1,k}$ within the kth layer. Therefore we can reduce the subscript of any photon flux from three elements to two. The first subscript remains to be i or s, referring to incident into or scattered away from the center of the sphere. However, the second element, k, only needs to refer to the layer that the photon flux is in. For example, as in Fig. 1(b), we assign $p_{s,k} \equiv p_{i,k,k} = p_{s,k-1,k}$ and $p_{i,k} \equiv p_{s,k,k} = p_{i,k-1,k}$. Accordingly, $p_{s,k+1} \equiv p_{i,k+1,k+1} = p_{s,k,k+1}$ and $p_{i,k+1} \equiv p_{s,k+1,k+1} = p_{i,k,k+1}$. Substituting $p_{s,k}$ for $p_{i,k,k}$, $p_{i,k}$ for $p_{s,k,k}$, $p_{s,k+1}$ for $p_{s,k,k+1}$, and $p_{i,k+1}$ for $p_{i,k,k+1}$ into Eqs. (4) and (5), we obtain the relationship of photon fluxes between the kth and the $(k + 1)$th layer in matrix form:

$$\begin{bmatrix} p_{i,k+1} \\ p_{s,k+1} \end{bmatrix} = \begin{bmatrix} \dfrac{\exp[i(\theta_k - \phi_k)]}{1 - R_k} & \dfrac{R_k \exp[i(\theta_k + \phi_k)]}{1 - R_k} \\ \dfrac{-R_k \exp[-i(\theta_k + \phi_k)]}{1 - R_k} & \dfrac{(1 - 2R_k)\exp[-i(\theta_k - \phi_k)]}{1 - R_k} \end{bmatrix} \times \begin{bmatrix} p_{i,k} \\ p_{s,k} \end{bmatrix}. \quad (8)$$

Subsequently, it can be proved that the incident and scattered photon fluxes $p_{i,j}$ and $p_{s,j}$ in any layer j can be related to the overall incident and scattered photon fluxes, $p_{i,N=1}$ and $p_{s,N+1}$, by the relation matrix as follows:

$$\begin{aligned} \begin{bmatrix} p_{i,N+1} \\ p_{s,N+1} \end{bmatrix} &= \begin{bmatrix} \dfrac{\exp[i(\theta_N - \phi_N)]}{1 - R_N} & \dfrac{R_N \exp[i(\theta_N + \phi_N)]}{1 - R_N} \\ -\dfrac{R_N \exp[-i(\theta_N + \phi_N)]}{1 - R_N} & \dfrac{(1 - 2R_N)\exp[-i(\theta_N + \phi_N)]}{1 - R_N} \end{bmatrix} \\ &\times \begin{bmatrix} \dfrac{\exp[i(\theta_{N-1} - \phi_{N-1})]}{1 - R_{N-1}} & \dfrac{R_{N-1} \exp[i(\theta_{N-1} + \phi_{N-1})]}{1 - R_{N-1}} \\ -\dfrac{R_{N-1} \exp[-i(\theta_{N-1} + \phi_{N-1})]}{1 - R_{N-1}} & \dfrac{(1 - 2R_{N-1})\exp[-i(\theta_{N-1} - \phi_{N-1})]}{1 - R_{N-1}} \end{bmatrix} \\ &\cdots \begin{bmatrix} \dfrac{\exp[i(\theta_j - \phi_j)]}{1 - R_j} & \dfrac{R_j \exp[i(\theta_j + \phi_j)]}{1 - R_j} \\ -\dfrac{R_{N-1} \exp[-i(\theta_{N-1} + \phi_{N-1})]}{1 - R_{N-1}} & \dfrac{(1 - 2R_j)\exp[-i(\theta_j - \phi_j)]}{1 - R_j} \end{bmatrix} \begin{bmatrix} p_{i,j} \\ p_{s,j} \end{bmatrix} \\ &= \begin{bmatrix} M_{11}^{(j)} & M_{12}^{(j)} \\ M_{21}^{(j)} & M_{22}^{(j)} \end{bmatrix} \begin{bmatrix} p_{i,j} \\ p_{s,j} \end{bmatrix}, \end{aligned} \quad (9)$$

where $M_{11}^{(j)}$, $M_{12}^{(j)}$, $M_{21}^{(j)}$, and $M_{22}^{(j)}$ are the components of the relation matrix.

Finally, the innermost layer, the mth layer, that the photon flux could reach can be obtained according to Eq. (6), under the condition of

$$\frac{r_N}{r_{m-1}}\frac{n_{N+1}}{n_m}\sin\theta_N \geq 1. \tag{10}$$

Obviously, the photon fluxes incident into the mth layer, will totally pass directly to the outer layer, which implies $p_{i,m} = p_{s,m}$. Thus according to Eq. (9), the overall scattered photon flux outside the sphere, $p_{s,N+1}$, can be related to the single incident ray $p_{i,N+1}$ as follows:

$$p_{s,N+1} = \frac{M_{21}^{(m)} + M_{22}^{(m)}}{M_{11}^{(m)} + M_{12}^{(m)}} p_{i,N+1}. \tag{11}$$

Furthermore, according to Eq. (1), it can be verified that the optical force $\mathbf{F}_{\text{ray}}$ induced by this single incident ray is

$$\mathbf{F}_{\text{ray}} = p_{i,N+1}\frac{h}{\lambda_{\text{med}}}\left[\text{Re}\left(1 - \frac{M_{21}^{(m)} + M_{22}^{(m)}}{M_{11}^{(m)} + M_{12}^{(m)}}\right)\hat{\mathbf{z}}' - \text{Im}\left(\frac{M_{21}^{(m)} + M_{22}^{(m)}}{M_{11}^{(m)} + M_{12}^{(m)}}\right)\hat{\mathbf{y}}\right], \tag{12}$$

where Re and Im are the operators of real and imaginary parts, respectively.

In the case of the optical force upon a uniform sphere, which is a special case of our multilayer sphere model, the overall scattered photon flux and induced optical force would be obtained by

$$p_{scat} = p_i\left\{1 + R\exp(-i2\theta) - \frac{(1-R)^2\exp[-2i(\theta-\phi)]}{1 + R\exp(2i\phi)}\right\}, \tag{13}$$

$$\mathbf{F}_{ray,1} = p_i\frac{h}{\lambda_{med}}\left(1 + R\cos 2\theta - \frac{(1-R)^2[\cos(2\theta-2\phi) + R\cos 2\theta]}{1 + R^2 + 2R\cos 2\phi}\right)\hat{\mathbf{z}}' + p_i\frac{h}{\lambda_{med}}\left(R\sin 2\theta - \frac{(1-R)^2[\sin(2\theta-2\phi) + R\sin 2\theta]}{1 + R^2 + 2r\cos 2\phi}\right)\hat{\mathbf{y}}'. \tag{14}$$

This result is exactly the same as that of Ashkin's work.[7]

B. Small Variant Condition

With Eq. (12), although the optical trapping force upon a multilayer sphere caused by a single ray is attainable, it is still not easy to obtain a simple guideline of the optical force induced by a single ray. For that reason, a further approximation will be useful. On the other hand, the variations of refractive indices of most biological cells are usually small, so a small variant condition would be valid to be introduced as an approximation here.[12] Under this condition, we consider the refractive index changes between layers to be small, and we only need to consider the effect of refractive index change to the terms of first order. Along with Fresnel's formula, it can be proved that the reflection rates between layers within the multilayer sphere are neglect. Consequently, it can be shown that a photon flux propagating from one layer to adjacent layers only changes its direction with a deflective angle, and the corresponding simplification of Eq. (9) would be shown as

$$\begin{bmatrix} p_{i,N+1} \\ p_{s,N+1} \end{bmatrix} \approx \begin{bmatrix} \frac{\exp[i(\theta_N - \phi_N)]}{1-R_N} & \frac{R_N\exp[i(\theta_N+\phi_N)]}{1-R_N} \\ -\frac{R_N\exp[-i(\theta_N+\phi_N)]}{1-R_N} & \frac{(1-2R_N)\exp[-i(\theta_N-\phi_N)]}{1-R_N} \end{bmatrix} \times \begin{bmatrix} \exp(i\Delta) & 0 \\ 0 & \exp(-i\Delta) \end{bmatrix}\begin{bmatrix} p_{i,m} \\ p_{s,m} \end{bmatrix}, \tag{15}$$

where Δ is the summation of the deflective angles of the photon fluxes within the multilayer sphere.

In addition, considering the refractive index distribution $n(r)$ as a continuous function of distance r from the center of the multilayer sphere, we also assume that the thickness of each layer is infinitely small, but the number of layers is infinitely large. Thus, the summation of the deflective angles in all interfaces Δ is given by

$$\Delta = \sum_{k=m}^{N-1}(\theta_k - \phi_k) \approx -\int_{r_m}^{r_N}\frac{\{dn_{med}/[rn^2(r)]\}n'(r)}{\sqrt{1 - \{dn_{med}/[rn(r)]\}^2}}\,dr. \tag{16}$$

Also, the scattered photon flux and the induced optical force will be obtained by

$$p_{s,N+1} \approx p_{i,N+1}\left(1 - R_N \exp(-i2\theta_N) + \frac{(1-R_N)^2 \exp\{-2i[\theta_N - (\phi_N - \Delta)]\}}{1 + R_N \exp[2i(\phi_N - \Delta)]}\right), \tag{17}$$

$$F_{ray} \approx p_{i,N+1}\frac{h}{\lambda_{med}}\left(1 + R_N \cos 2\theta_N - \frac{(1-R_N)^2\{\cos[2\theta_N - 2(\phi_N - \Delta)] + R_N \cos 2\theta_N\}}{1 + R_N{}^2 + 2R_N \cos[2(\phi_N - \Delta)]}\right)\hat{\mathbf{z}}'$$
$$+ p_{i,N+1}\frac{h}{\lambda_{med}}\left(R_N \sin 2\theta_N - \frac{(1-R_N)^2\{\sin[2\theta_N - 2(\phi_N - \Delta)] + R_N \sin 2\theta_N\}}{1 + R_N{}^2 + 2R_N \cos[2(\phi_N - \Delta)]}\right)\hat{\mathbf{y}}'. \tag{18}$$

Comparing Eq. (13) with Eq. (17), and Eq. (14) with Eq. (18), it can be observed that under a small variant condition, the approximate formulas upon a nonuniform sphere are similar to the ones upon a uniform sphere. The reflection rate R at the boundary of the sphere and the initial incident angle θ remain the ones upon the multilayer sphere, R_N and θ_N, respectively. The only difference is that refractive angle ϕ in the uniform sphere model is replaced by $(\phi_N - \Delta)$.

C. Optical Force Induced by Focused Rays

Based on the optical force induced by one ray in Eqs. (14) and (18), we can attain the optical force caused by a focusing laser beam by summing the effects of the whole bundle of rays. We consider a bundle of parallel incident rays propagating through a focusing lens and then focused to a point, as shown in Fig. 2. Also, the direction of the ray can be described as $(\sin\Theta\cos\Phi, \sin\Theta\sin\Phi, \cos\Theta)$. Assuming that the center of a multilayer sphere locates at coordinates (x_0, y_0, z_0), the distance vector from the center of the sphere to the incident ray, $\mathbf{d}$, can hence be shown as follows:

$$\begin{aligned}\mathbf{d} = {} & [-x_0(\cos^2\Theta + \sin^2\Theta\sin^2\Phi) \\ & + y_0(\sin^2\Theta\cos\Phi\sin\Phi) \\ & + z_0(\cos\Theta\sin\Theta\cos\Phi)]\hat{\mathbf{x}} \\ & + [x_0(\sin^2\Theta\cos\Phi\sin\Phi) - y_0(\cos^2\Theta \\ & + \sin^2\Theta\cos^2\Phi) + z_0(\cos\Theta\sin\Theta\sin\Phi)]\hat{\mathbf{y}} \\ & + [x_0(\cos\Theta\sin\Theta\cos\Phi) + y_0(\cos\Theta\sin\Theta\sin\Phi) \\ & - z_0\sin^2\Theta]\hat{\mathbf{z}}. \end{aligned} \tag{19}$$

Comparing Fig. 2 with Fig. 1(a), for every ray, the direction of the ray and the distance vector $\mathbf{d}$ is along $\hat{\mathbf{z}}'$ and $\hat{\mathbf{y}}'$, respectively. Consequently, it can be shown that the total force induced by the focused rays is given by

$$\mathbf{F}_{tot} = \int_0^{2\pi}\int_0^{\Theta_m} \mathbf{F}_{ray} \times [p_i(\Theta, \Phi), \hat{\mathbf{z}}'(\Theta, \Phi), \mathbf{d}(\Theta, \Phi), n(r)]\mathrm{d}\Theta\mathrm{d}\Phi, \tag{20}$$

where r is the distance from the center of the multilayer sphere, $n(r)$ is the distribution of the refractive index, and Θ_m is the maximum value of Θ, which is limited by the numerical aperture (N.A. = $n_{med}\sin\Theta_m$) of the focusing lens.

In addition, optical tweezers are conventionally analogous to a three-dimensional (3D) optical spring. According to Eq. (20), to the first-order approximation of (x_0, y_0, z_0), the transverse and longitudinal components of the stiffness of the 3D optical spring is given by

$$k_x = k_y = \left.\frac{\partial F_{tot,x}}{\partial x_0}\right|_{(0,0,0)} = \left.\frac{\partial F_{tot,y}}{\partial y_0}\right|_{(0,0,0)}, \tag{21}$$

$$k_z = \left.\frac{\partial F_{tot,z}}{\partial z_0}\right|_{(0,0,0)}, \tag{22}$$

respectively.

3. Numerical Results

A. Data of Refractive Indices and Sizes of Chinese Hamster Ovary Cells

Recently, detailed refractive indices of organelles and bacterial cells have been rarely characterized. A rough estimate of the refractive index of mammalian cells, which we also referred to in our last work, is in

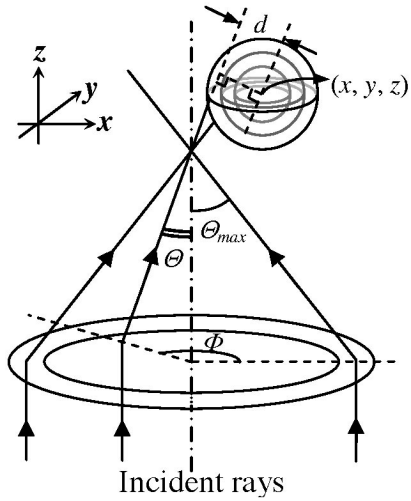

Fig. 2. Schematic of a bundle of rays focused at the origin point and their relative locations with a multilayer sphere.

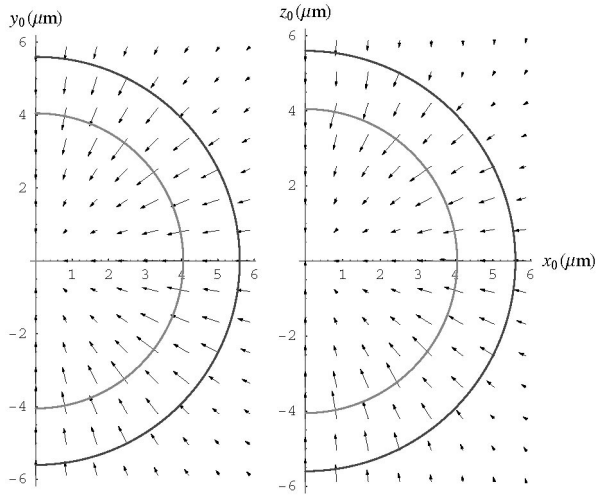

Fig. 3. Magnitude and direction of the optical force upon a CHO cell in the *XY* and *XZ* planes.

Brunsting and Mullaney's work.[14] They modeled the CHO cell as a coated sphere in an optical and morphological fashion. In their model, the nucleus of the mammalian cell is surrounded by its cytoplasm.

In their measurement, the magnitudes of the refractive index of the cytoplasm, n_{cyt}, and the refractive index of the nucleus, n_{nuc}, were measured to be 1.3703 and 1.392 $\pm$ 0.005, respectively. Also, they found a linear relationship between the radius of the nucleus, r_{nuc}, and the radius of the cell, r_{cell}, for many CHO cells of various sizes as given by

$$r_{cell} = (1.38 \pm 0.02) r_{nuc} + (0.03 \pm 0.05). \quad (23)$$

On average, the magnitudes of $\langle r_{nuc} \rangle$ and $\langle r_{cell} \rangle$ were measured to be 4.05 $\pm$ 0.45 and 5.60 $\pm$ 0.25 μm, respectively. As a comparison, we took another virtual CHO cell of the same size with a uniform refractive index of 1.379 as an example of a uniform sphere to our cell-like model. Note that the value of 1.379 is the averaged refractive index of the CHO cell.

B. Numerical Analysis

With our method, it is valid to calculate the optical force upon a biological cell around the focus of the focusing laser. Figure 3 shows a field plot of the optical force upon a CHO cell whose size and refractive index distribution are mentioned above, when the center of the CHO cell is in the *XY* and *XZ* planes. Also, the gray circles in Fig. 3 label the radius of the nucleus of the CHO cell and the radius of the whole cell, individually. Additionally, in this exercise, we assume that the cell is trapped in water, and that the cell's refractive index is 1.33. Also, the optical tweezer system is assumed to consist of a 1 mW laser and a microscope objective of 1.25 N.A., and the intensity of the focusing laser rays in different directions is also assumed to be uniform.

The validity of our model is also numerically examined by comparing the difference in magnitude between the optical forces upon a uniform sphere and the ones for a nonuniform cell of the same size. In this exercise, we take the uniform virtual CHO cell with a uniform refractive index of 1.379 as an example of a uniform sphere, and a CHO cell seems to be a sufficient example of the nonuniform cell. As shown in Fig. 4(a), under the same optical tweezers system condition as discussed above, the *x* component of the optical force upon uniform and nonuniform cells with a relative displacement along the *x* axis between the laser focus of the optical tweezers and the centers of the cells are indicated. Additionally, the optical force upon the CHO cell is calculated both with an exact method and with an approximation under a small variant condition. Similar simulations of the *z* component of the optical forces versus the relative displacement along the *z* axis are also shown in Fig. 4(b).

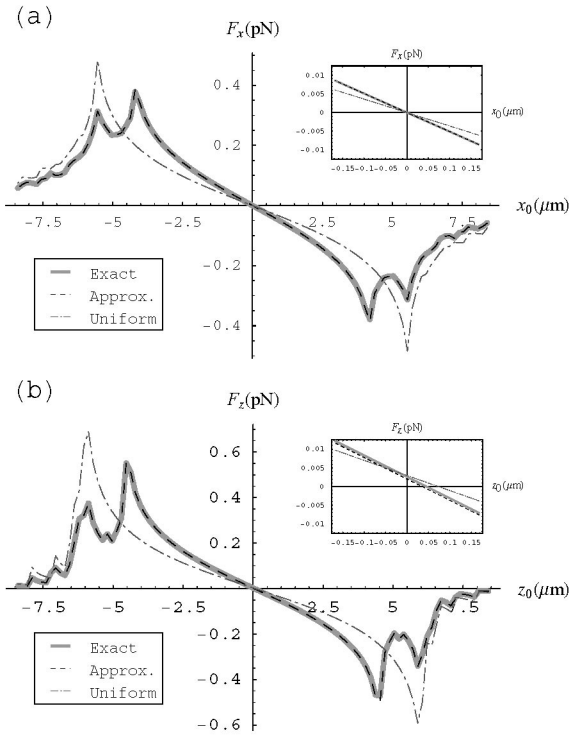

Fig. 4. Optical force versus the displacements of trapped uniform and nonuniform cells showing (a) the relationships between the *x* component of optical force and the displacements on the *x* axis of the trapped CHO cells, and (b) the ones between the *z* component of optical force and the displacements on the *z* axis. The gray curve and dashed curve represent the numerical results of nonuniform cells with the exact matrix method and with approximation under a small variant condition, respectively. The dashed-point curve represents the numerical result of a uniform virtual cell.

The stiffness of the optical tweezers is also simulated. In this exercise, other than the uniform virtual CHO cell, a silica bead and a polystyrene bead are also ideal to use as uniform spheres, because they are often used in cellular and molecular biology experiments with optical tweezers. For sure, the radii of the two beads are taken to be the same as that of the CHO cell, which is 11.2 μm. Note that the refractive

Table 1. Numerical Results of Stiffness[a]

	Nonuniform CHO Cell		Uniform Virtual CHO Cell	Silica Bead	Polystyrene Bead
	Accurate Result (Matrix Calculation)	Approximate Result (Small Variant Condition)			
Refractive index	$n_{max} = 1.392$ ($0 \le r < 4.05 \pm 0.45$ μm) $n_{cyt} = 1.3703$ (4.05 ± 0.45 μm $\le r \le 5.60 \pm 0.25$ μm)		1.379	1.45	1.56
Transverse stiffness, k_x and k_y (10^{-9} Nt/m)	50.97±2.27	50.98±2.28	36.01	83.35	143.71
Longitudinal stiffness, k_z (10^{-9} Nt/m)	57.19±2.55	57.21±2.56	40.39	93.53	163.60

[a]The transverse and longitudinal stiffness of optical trapping upon four 11.2 μm radius samples including a nonuniform virtual CHO cell, a uniform virtual CHO cell, a silica bead, and a polystyrene bead, which are caused by an optical tweezers system using a 1 mW laser and a 1.25 N.A. objective lens.

indices of the uniform silica bead and polystyrene bead are 1.45 and 1.56, respectively.

By substituting the appropriate values into Eqs. (21) and (22) for transverse and longitudinal stiffness of optical tweezers upon the nonuniform CHO cell of 11.2 μm diameter, we obtain exact and approximate solutions as follows: the transverse stiffness is approximately 50.97×10^{-9} Nt/m, and the longitudinal stiffness is approximately 57.20×10^{-9} Nt/m, separately. Similarly, we obtain the ones for the uniform virtual CHO cell, the silica bead, and the polystyrene bead, respectively. All the data for the two kinds of virtual CHO cell, the silica bead, and the polystyrene bead are listed in Table 1.

4. Discussion

According to the simulation results in Section 3, the relationship between the optical force and the relative displacement between the laser focus and a trapped particle in a nonuniform cell case is much different from the one in a uniform sphere case. It can be seen that in the case of a uniform sphere, the optical force increases with the increase of the relative displacement of the trapped sphere until the laser focus is outside the sphere, as shown in Fig. 4. Obviously, there is only one maximum in the optical force curve. This phenomenon agrees with Ashkin's work.[7] However, in the case of a nonuniform cell, there are two local maxima in the optical force curve as shown in Figs. 3 and 4. Further investigation shows that the two maxima appear when the relative displacement is around the radius of the nucleus and the radius of the whole cell, separately. This twin-peak phenomenon has not been predicted in a conventional ray-optics model.

To clarify the twin-peak phenomenon in our exercise of the nonuniform cell, we should investigate how a local maximum occurs. As we recall, the optical force in the ray-optics regime is generated due to momentum transfer between photons and the trapped particle. When the incident angles of most rays propagate into an interface near 90°, the corresponding deflected angles of the refracted rays reach their maxima, according to Snell's law. This leads to maximum momentum transfer, which results in a maximum optical force. Therefore in both cases of uniform and nonuniform cells, a local maximum optical force appears as the laser focus is at the edge of a trapped particle, the interface between the cell, and the surrounding medium. Similarly, in the case of a nonuniform cell, the two-layer CHO cell case, the other maximum optical force will appear as the laser focus is near the interface between the nucleus and the cytoplasm.

On the other hand, we have compared the magnitudes of the stiffness simulated by the approximation method under a small variant condition and an exact method, as shown in Fig. 4 and Table 1. It can be seen that the difference between the approximate result and the exact one is less than 1%. This proves that the approximation under a small variant condition is sufficient enough to calculate the optical force upon biological cells in the ray-optics regime.

Also, it can be seen in Table 1 that the stiffness of the optical tweezers upon a silica bead and upon a polystyrene bead is approximately 1.7–2.9 times that of a CHO cell. This predication agrees with the experimental result of Liang *et al.*[15] They found that the trapping force upon a polystyrene bead is three times that upon an *Escherichia coli* cell. Similarly, we also found in our measurement that the trapping force upon a 1 μm diameter polystyrene bead is approximately 3.8 times that upon a *K. Pneumoniane* cell, whose long axis is 1.2 μm and short axis is 0.98 μm. It is worth noting that even though the sizes and shapes of uniform beads and *E. coli* and *K. Pneumoniane* cells are not really in the ray-optics regime, a similar relationship of the trapping forces among them remains the same.

5. Conclusion

We have successfully developed a model to estimate the optical force upon a biological nonuniform cell, which is expanded from Ashkin's ray-optics model for a uniform sphere. First, we assume the cell to be a multilayer sphere with a spherically symmetric refractive index. Then we calculate the optical force from the momentum-transfer rate of the laser beam.

This model only requires the radial distribution of the refractive index of the cell and the distribution of intensity of the focusing laser beam to obtain the optical force versus the displacement between the laser focus and the center of the biological cell. As a result, we can acquire the stiffness of the trapping force upon the biological cell.

A numerical simulation of this model also shows that the force upon a nonuniform biological cell is much different from that upon a uniform sphere. It can be proved that the optical force upon a trapped cell apparently depends on the distribution of the refractive index of the cell.

On the other hand, we also derive an approximation of this model under a small variant condition. In this approximation, the formulas are actually the ones in a conventional ray-optics model with the reflective rates and deflective angles slightly adjusted. The difference between the approximate result and the exact one is less than 1%.

References

1. A. Ashkin, J. M. Dziedzic, J. E. Bjorkholm, and S. Chu, "Observation of a single-beam gradient force optical trap for dielectric particles," Opt. Lett. **11,** 288–290 (1986).
2. S. C. Grover, A. G. Skirtach, R. C. Gauthier, and C. P. Grover, "Automated single-cell sorting system based on optical trapping," J. Biomed. Opt. **6,** 14–22 (2001).
3. M. Ozkan, T. Pisanic, J. Scheel, C. Barlow, S. Esener, and S. N. Bhatia, "Electro-optical platform for the manipulation of live cells," Langmuir **19,** 1532–1538 (2003).
4. M. Ozkan, M. Wang, C. Ozkan, R. Flynn, A. Birkbeck, and S. Esener, "Optical manipulation of objects and biological cells in microfluidic devices," Biomed. Microdevices **5,** 61–67 (2003).
5. Y. Wakamoto, I. Inoue, H. Moriguchi, and K. Yasuda, "Analysis of single-cell differences by use of an on-chip microculture system and optical trapping," Fresenius J. Anal. Chem. **371,** 276–281 (2001).
6. G. Hummer and A. Szabo, "Free-energy reconstruction from nonequilibrium single-molecule pulling experiments," Proc. Natl. Acad. Sci. U.S.A. **98,** 3658–3661 (2001).
7. A. Ashkin, "Forces of a single-beam gradient laser trap on a dielectric sphere in the ray optics regime," Biophys. J. **61,** 569–582 (1992).
8. Y. Harada and T. Asakura, "Radiation forces on a dielectric sphere in the Rayleigh scattering regime," Opt. Commun. **124,** 529–541 (1996).
9. J. P. Barton, D. R. Alexander, and S. A. Schaub, "Theoretical determination of net radiation force and torque for a spherical particle illuminated by a focused laser beam," J. Appl. Phys. **66,** 4594–4602 (1989).
10. F. Ren, G. Grehan, and G. Gouesbet, "Radiation pressure forces exerted on a particle located arbitrarily in a Gaussian beam by using the generalized Lorentz-Mie theory, and associated resonance effects," Opt. Commun. **108,** 343–354 (1994).
11. A. Rohrbach and E. H. K. Stelzer, "Optical trapping of dielectric particles in arbitrary fields," J. Opt. Soc. Am. A **18,** 839–153 (2001).
12. R. C. Gauthier, "Computation of the optical trapping force using an FDTD based technique," Opt. Express **13,** 3707–3718 (2005).
13. Y.-R. Chang, L. Hsu, and S. Chi, "Optical trapping of a spherically symmetric Rayleigh sphere: a model for optical tweezers upon cells," Opt. Commun. **246,** 97–105 (2005).
14. A. Brunsting and P. F. Mullaney, "Differential light scattering from spherical mammalian cells," Biophys. J. **14,** 439–453 (1974).
15. M. N. Liang, S. P. Smith, S. J. Metallo, I. S. Choi, M. Prentiss, and G. M. Whitesides, "Measuring the forces involved in polyvalent adhesion of uropathogenic *Escherichia coli* to mannose-presenting surfaces," Proc. Natl. Acad. Sci. U.S.A. **97,** 13092–13096 (2000).